JOURNAL OF MATERIALS SCIENCE 7 (1972) 220–238

The Formation and Microstructure of Dental Silicate Cements

A. D. WILSON, B. E. KENT
Laboratory of the Government Chemist, Cornwall House, Stamford Street, London SE1, UK

D. CLINTON, R. P. MILLER
Division of Inorganic and Metallic Structure, National Physical Laboratory, Teddington, Middlesex, UK

The chemistry of the cement-forming reaction between phosphoric acid solutions and fluorine-containing aluminosilicate glasses has been studied using a variety of physico-chemical methods. These materials are the dental silicate cements and the microstructures of a number of these cements have been examined by optical, electron and scanning electron microscopy. The element distribution between partially reacted glass particles and the gel matrix which binds them has been determined by electron probe microanalysis.

The chemical stability and variations in the mechanical strength between different cements is discussed in terms of a new hypothesis on the constitution of the gel matrix. Consideration is given to the possible strengthening role of microcrystallinity which has been shown by X-ray and electron diffraction to develop in the matrix. Attempts to strengthen the cement by incorporation of reinforcing agents is described.

1. Introduction

The most commonly used material for the restoration of anterior teeth is the dental silicate cement which is the product of a reaction between a powdered fluorine-containing aluminosilicate glass and a phosphoric acid solution [1, 2]. The cement paste sets and hardens within a few minutes in the mouth, developing a compressive strength which has been known to attain a value of 300 MN/m^2 (44000 psi) in 24 h. The set cement is translucent, enabling it to be matched to tooth enamel in appearance, a primary requirement for any anterior filling material. Other advantages are a thermal expansion which matches that of dentine and tooth enamel, a cariostatic action attributed to the cement's ability to slowly release fluoride ions, and a good resistance towards abrasion.

The chief disadvantage of this cement is the staining, erosion and ultimate disintegration it undergoes in oral fluids, so that restorations made from it cannot be considered truly permanent. There are also important limitations in applications because of the brittle nature of this material.

The life of a dental silicate cement is highly variable; while a few last 25 years, some fail within months and the average life has been estimated as only four to five years. In spite of its failure in the mouth this cement remains the most popular anterior restorative material and there are about forty brands on the world market. Thus it is important to understand the reasons for their failure in clinical use, to optimise preparative conditions and to assess whether they are capable of significant improvement.

The purpose of this paper is to review the physical and chemical changes which have been observed during the setting and hardening processes; to examine the microstructure of set cements and the element distribution in them; and to attempt to relate variations in strength with the nature of the microstructure. The results will also be given of a brief study of the feasibility of strengthening by reinforcement with carbon or silicon carbide whiskers and by alumina particles.

2. Experimental

2.1. Materials

Brands of cement examined were coded by numbers, as in table I. Letter prefixes P, L and C

TABLE I Commercial dental silicate cements.

Number	Brand	Manufacturer
1	Syntrex	Amalgamated Dental Co, London, England
2	Super Syntrex	Amalgamated Dental Co, London, England
4	New Filling Porcelain	S. S. White Dental Manufacturing Co, Harrow, England
6	Achatit	Vivadent, Schaan, Liechtenstein
8	True Shade	Dental Fillings Ltd, London, England
9	Astralit	Dental Fillings Ltd, London, England
10	Terralux	Zahn-Porzellan K.G., Hamburg, Germany
11	Terralux Ultra	Zahn-Porzellan K.G., Hamburg, Germany
12	Plastic Filling Porcelain	Baker Platinum Division, London, England
13	Synthetic Enamel	Lee Smith Co, Chicago, USA
14	Fiberin	Lee Smith Co, Chicago, USA
15	Dralalith	Drala GmbH, Hamburg, Germany
16	Translucin	Drala GmbH, Hamburg, Germany
17	Ames Plastic Porcelain	W.V-B., Ames Co, Fremont, Ohio, USA
18	Porsilon	Odus Dental A.G. Dietikon, Zürich, Switzerland
19	Diafil	Pfingst and Co, Inc, New York, USA
20	Super Diafil	Pfingst and Co, Inc, New York, USA
28	Omnifil	Jota Dental und Schleifmittel GmbH, Düsseldorf, Germany
29	Achatit Biochromatic	Vivadent, Schaan, Liechtenstein
35	Harvard-Cement (quick-setting)	Richter and Hoffmann, Harvard Dental Ges, W. Berlin, Germany
41	Harvard Crystone	Richter and Hoffmann, Harvard Dental Ges, W. Berlin, Germany
42	Luxsilit	DMG Dental Material, GmbH, Hamburg, Germany
44	Biotrey	Amalgamated Dental Co, London, England

in subsequent tables refer to the powder, liquid and cement respectively.

2.1.1. Powder composition

Seventeen currently available powders were examined and all found to contain silicon, aluminium and fluorine as major constituents, together with smaller amounts of sodium and calcium, and in all but two cases, phosphorus. All powders were substantially amorphous as assessed by X-ray diffraction and the conclusion was drawn that they were ground fluorine-containing aluminosilicate glasses. Chemical analyses of some typical powders are given in table II. One general conclusion to be drawn from these data, taken together with those of Axelsson [3], is that the dental silicate glass is characterised by a Si:Al mole ratio of approximately unity, suggesting that the glass network may be nominally represented as a negatively charged three-dimensional framework of linked $[SiO_4)$ and $[AlO_4]$ tetrahedra.

The F:Si ratio is higher than in any formulation recorded for opal glasses and it will be demonstrated later that the glasses are phase-separated. In P-6, P-8 and P-11 minor amounts of crystalline fluorite and quartz were detected by X-rays. It is understood that, commercially, the glasses are prepared by fusing appropriate quantities of quartz, silica and alumina in a cryolite/fluorite flux containing small quantities of phosphate.

Particle size distribution curves for two typical powders P-2 and P-8 are shown in fig. 1. Two powders were found to contain glass fibres, P-6 for example included 2 wt % of fibres mainly 2 mm long.

2.1.2. Liquid composition

The chemical analyses of a range of commercial liquids are set out in table III. The concentration of phosphoric acid varied from 46 to 66% H_3PO_4. All commercial liquids contained metals, commonly aluminium and zinc, which are required to be soluble in phosphoric acid, non-toxic and incapable of forming coloured sulphides. It has been demonstrated elsewhere [4-6] that whereas zinc is in simple solution, aluminium forms complexed bridged structures with phosphoric acid. The compositions of experimental liquids, P, PA and PAZ-types, used throughout the study are also given in table III.

TABLE II Chemical composition of glass powders*.

	P-2	P-4	P-6	P-8	P-11
SiO_2	41.6	38.8	31.5	34.5	35.9
	(0.693)	(0.647)	(0.525)	(0.575)	(0.598)
Al_2O_3	28.2	29.1	27.2	28.3	29.0
	(0.276)	(0.285)	(0.267)	(0.277)	(0.284)
CaO	8.8	7.7	9.0	8.5	6.1
	(0.157)	(0.138)	(0.161)	(0.152)	(0.109)
Na_2O	7.7	8.2	11.2	11.2	14.5
	(0.124)	(0.133)	(0.181)	(0.181)	(0.233)
F	13.3	13.8	22.0	18.1	15.2
	(0.700)	(0.726)	(1.157)	(0.953)	(0.800)
P_2O_5	3.3	3.0	5.3	3.3	4.4
	(0.023)	(0.021)	(0.037)	(0.023)	(0.031)
ZnO	0.3	2.9	—	0.1	0.3
	(0.004)	(0.036)		(0.001)	(0.004)
H_2O	2.2	1.6	—	1.7	1.4
	(0.120)	(0.089)		(0.095)	(0.078)
Less O for F	− 5.6	− 5.8	− 9.3	− 7.6	− 6.4
Total	99.8	99.4	96.9	98.1	100.4

*Given as per cent by weight.
Mole ratios given in brackets ( ).

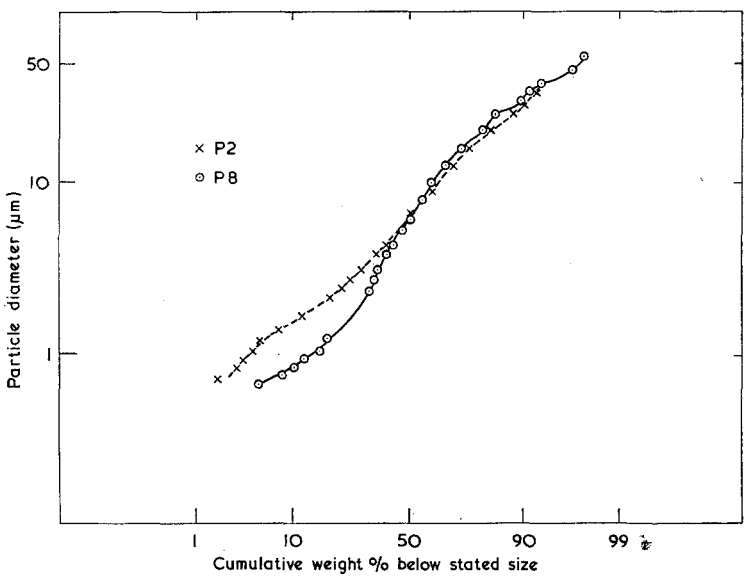

Figure 1 The particle-size distribution of two brands of dental silicate cements, P-2 and P-8.

2.1.3. Cement preparation

Cements were prepared at 23 ± 1°C by spatulating a weighed amount of powder (along with any filler) with a known volume of liquid on a glass slab using the technique prescribed in the international specification for dental silicate cement [7]. Typical compositions of cements are given in table IV. The ratio of powder to liquid normally selected was such that it yielded a cement paste having a standard consistency as defined and determined in the international specification for this cement [7]. Typical values of this ratio are given in table V.

2.1.4. Cement properties

Compressive strength, setting time and solubility

TABLE III Chemical composition of liquids.

Liquid	Commercial liquids				
	Phosphoric acid (H_3PO_4 wt %)	Aluminium (Al wt %)	Zinc (Zn wt %)	Magnesium (Mg wt %)	Beryllium (Be wt %)
L-1	48.3	2.3	4.9	—	—
L-2	48.8	1.6	6.1	—	—
L-4	49.3	1.9	4.2	—	—
L-6	50.7	1.5	8.7	—	—
L-8	55.5	2.0	9.1	—	—
L-9	49.1	2.0	5.0	—	—
L-10	65.8	1.8	—	1.3	—
L-11	65.9	—	—	1.6	0.65
L-12	65.0	1.4	1.5	0.4	—
L-13	48.0	—	8.4	—	—
L-14	48.2	—	8.4	—	—
L-15	52.7	—	2.4	0.3	—
L-16	54.3	—	2.4	0.3	—
L-17	45.9	2.2	5.3	—	—
L-18	51.9	2.5	5.5	—	—
L-19	48.7	—	6.9	1.1	—
L-20	48.5	—	7.9	1.1	—
	Experimental liquids				
P-type	49.0x	—	—	—	—
P-O	49.0	—	—	—	—
PAZ-type	49.0x	1.25x	6.0x	—	—
PAZ-0	49.0	1.25	6.0	—	—

where x values from 0.6 to 1.5

TABLE IV Composition of cements.

Sample No.	P_2O_5		Al_2O_3		SiO_2		CaO		Na_2O		F		ZnO		H_2O	
	wt %	mol ratio	wt %	mol ratio	wt %	mol ratio	wt %	mol ratio	wt %	mol ratio	wt %	mol ratio	wt %	mol ratio	wt %	mol ratio
C-11	21.1	0.149	18.2	0.178	22.2	0.370	3.8	0.068	9.1	0.147	9.5	0.500	0.2	0.002	18.8	1.042
C-6	15.0	0.106	19.7	0.193	21.8	0.364	6.3	0.113	7.8	0.126	15.2	0.800	3.6	0.044	18.5	1.030
C-2	12.5	0.088	20.8	0.204	29.6	0.493	6.3	0.113	5.5	0.089	9.5	0.500	2.4	0.030	16.9	0.940

for the unreinforced cements were determined by the international specification tests [7]. Young's moduli and moduli of rupture of the reinforced cements were determined using an Instron Universal Testing Instrument. The specimens for these tests were prepared by spatulations of the glass powder, with the filler, at different phosphoric acid powder to liquid ratios and the mixes allowed to set in moulds.

Hardness was determined by measuring the depth of indentation of a standard Vickers diamond into a cement surface using a Wallace Hardness Tester. Hardness was recorded as Woxen Hardness number (g cm^{-2}) calculated from the indentation [8].

2.1.5. pH changes

These were measured by embedding a flat-headed glass electrode in the cement paste immediately after mixing, and taking pH readings during setting and hardening.

2.2. Electron Probe Microanalysis (EPMA) (with Miss D. Poynter*)

Fragments of the original uncrushed glass from which P-2 is prepared were crushed and sieved,

*Warren Spring Laboratory, Department of Trade and Industry, Stevenage, Herts, UK.

TABLE V Physical properties of dental silicate cements*.

Cement	Powder/liquid ratio g ml^{-1}	Resistance to compression (MN m^{-2})	Setting time (min)	Solubility and disintegration (%)
C-2	4.00	304	3¾	0.44
C-4	3.90	255	3½	0.50
C-5	3.90	198	3¼	0.58
C-6	4.10	252	3¾	0.42
C-8	3.10	166	7	0.71
C-9	4.10	243	5	0.63
C-11	2.70	68.5	5¾	3.8
C-17	4.10	250	3¾	0.40
C-19	3.00	213	3½	0.62
C-20	3.50	304	—	0.34
C-28	3.30	100	3½	1.80
C-29	3.60	214	4½	0.41
C-35	3.50	181	4¼	0.77
C-41	3.75	138	4¾	0.80
C-42	3.50	225	4½	0.97
C-44	4.02	256	3½	0.40
*Specification requirements [4]:		163	3-8	1.0

and a coarse fraction of particle size 45 to 105 μm containing no fine powder was selected for cement preparation. Cements were prepared using 49% H_3PO_4 solutions containing no metal ions. This was to avoid confusion due to aluminium present in commercial liquids.

A large fragment of the fully hardened dental cement was impregnated with a cold-setting epoxy resin and the sample was ground so as to expose a flat surface of the cement. This was polished using $\frac{1}{4}\mu$m diamond paste in oil. It was necessary for the sample to be vacuum-coated with a conducting layer of carbon, of which a 200Å layer was thick enough to be electrically conducting, yet thin enough to remain optically transparent.

A Cambridge Geoscan electron probe microanalyser was used for this investigation, with a flow proportional counter as a detector. The elements were excited using an accelerating voltage of 12 keV, a constant specimen current of about 20 nanoamperes (nA) being maintained throughout the study.

2.3. Optical Microscopy

Petrographic thin sections for examination in transmitted light were prepared by glueing pieces of cement to a glass slide, grinding, and polishing with successive sizes of carborundum (20 to 40 μm).

For observations using incident light, specimens were mounted in a cold-setting resin and the surface ground, using successive sizes of a diamond abrasive compound. Surfaces were then etched for 5 sec with 0.5 HF solution. A Reichardt microscope with a Nomarski attachment was used for observations under reflected light.

2.4. Electron Microscopy

Thin sections for examination in transmission were prepared by grinding sections of cement to approximately 20 μm thickness and then ion-thinning the wafers in an Edwards Ion Beam Machine to submicron thicknesses.

Carbon/platinum replicas were difficult to produce from fracture surfaces so single-stage replicas were taken from the surfaces of specimens mounted, ground, polished and etched in the manner described in section 2.3. Before depositing the carbon/platinum film by the usual evaporating techniques, the surface of the cement was coated with a film of silver which, by its ready solubility in dilute HNO_3, enabled the C/Pt replica to be easily removed from the surface. Extraction replicas were taken by a two-stage process. Acetylcellulose plastic was laid on a fractured surface, peeled off, and the film coated with carbon. The plastic was then dissolved in methyl acetate leaving the carbon replica and any adhering particles.

Most of the work on replicas was done using a JEOL JEM 7 electron microscope but in the latter part of the investigation the million volt AEI EM7 microscope became available and was used for transmission studies.

The Cambridge Stereoscan scanning electron

microscope was used to examine surfaces fractured in tension and etched for 5 sec with 0.05% HF.

2.5. X-Ray Powder Diffraction

Photographs were taken using a Phillips 11.4 cm camera using CuKα radiation. In some cases it was necessary to use exposures of 10 h to obtain a spectrum of reasonable intensity.

3. Results

3.1. Properties of Cements

Many of the data discussed in this section and the next are drawn from the published work of Wilson *et al* [6, 9-14].

The properties of a number of brands, coded here by C numbers, are summarised in table V. All were mixed to a standard consistency and it is noticeable that the powder/liquid ratio required to attain this varies markedly, from 2.7 to 4.1 g ml^{-1}. Setting times are all within specification but there is considerable variation in "solubility and disintegration" (from 0.34 to 3.8%) and in compressive strength (from 68.5 to 304 MN m^{-2}). The cement C-11 is of particular interest inasmuch as it possessed the worst properties and was the subject of a published adverse report by the Council on Dental Research [15]. For this reason it has been singled out for more extensive subsequent examination.

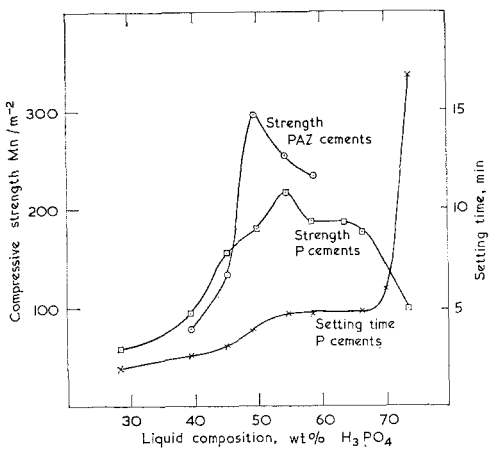

Figure 2 The effect of liquid composition on cement strength and setting time (P-2). Liquids used are the experimental ones shown in table III.

The effect of liquid composition on cement property is presented in fig. 2. The H_3PO_4:H_2O ratio is shown to have a critical influence on cement strength; the well defined optimum H_3PO_4 concentration for maximum strength depends on the presence or absence of aluminium and zinc. Setting time increases rapidly with the H_3PO_4:H_2O ratio for concentrations greater than 65 wt % H_2PO_3 and this may be attributed to (a) the changes in structure of phosphoric acid; (b) deficiency of water for the reaction; and (c) hydration of reaction products. The influence of the powder: liquid ratio on cement property is shown in table VI.

TABLE VI Effect of powder/liquid ratio on compressive strength and setting time (cement C-2).

Powder/liquid ratio g ml^{-1}	Resistance to compression (MN m^{-2})	Setting time (min)
2.5	—	24
2.75	—	10
3.0	220	$6\frac{3}{4}$
3.5	240	$4\frac{1}{2}$
4.0	325	$3\frac{1}{4}$
4.5	325	3

3.2. Cement Formation

The variation in the soluble ion content of a cement paste (C-2) in the period following preparation is shown graphically in fig. 3. The form of the curve indicates that Na^+, Ca^{2+}, Al^{3+} and F^- ions are liberated from the glass and, with the exception of Na^+, which is assumed to be readily soluble in excess water, are fixed in the cementing matrix by a type of precipitation process which will be discussed more fully later. It is evident from fig. 3 that the decomposition of the powdered glass is rapid since, at the observed point corresponding to the completion of mixing, appreciable amounts of the ions originally in the glass have been liberated.

If it is assumed that the total amount of sodium leached is a measure of the extent to which the glass has reacted, it is found that 10% of the glass has been attacked at the completion of mixing, an amount which ultimately rises to 20%. It is clear therefore from this and the microstructural studies described later that the bulk of the glass remains as an unattacked aggregate.

A similar study was undertaken using cement C-11 where calculation showed that a much greater proportion of the powder, 44%, was attacked. This difference is explained by the lower powder/liquid ratio of the cement paste (2.7 g ml^{-1} compared with 4.0 g ml^{-1} for C-2,

see table V) and the higher phosphoric acid concentration of the liquid (65.9% compared with 48.8%). Calculation shows that the powder/phosphoric acid weight ratio is 2.8 g ml^{-1} for C-11 compared with 5.3 g ml^{-1} for C-2.

The consequence is that the ratio of aggregate: gel matrix is much lower in C-11. Since these may be regarded as composite materials where the glass particles reinforce the cementing matrix, the comparative weakness of C-11 may be a reflection of this lower ratio.

It has also been shown that the amount of sodium liberated from C-11 is 4.7 times greater than that liberated from C-2 for a given quantity of powder. Thus the set cement C-11 contains far greater amounts of soluble sodium salts. This explains (1) its high solubility, and (2) the absorption of water by the cement due to osmotic forces, which can result in spontaneous disintegration.

The course of the setting and hardening processes have also been followed by infra-red total reflectance spectroscopy, electrical conductivity, apparent pH change and Woxen hardness measurements, and leaching studies, the data being plotted in fig. 4 as a function of the age of the cement (C-2). After set, which is not reflected by any sharp discontinuity in electrical conductivity, pH or soluble ion versus time curves, the chemical and physical changes continue. Hardness develops rapidly, reaching 65% of its maximum within 30 min after preparation. Hardening is accompanied by decreases in electrical conductivity, in soluble ion content and by increase in recorded pH. After setting, little further extraction of sodium from the cement occurs and no further changes in extractable sodium could be detected after 30 min, a result which is taken to indicate that at this stage major interaction has ceased between the glass powder and liquid.

The increase in hardness parallels the rise in recorded pH from 2.5 to 5.5. The ultimate values are reached in 72 h although there is little increase after 24 h. No further precipitation of ions could be detected after 48 h.

The changes after 30 min must be the result of further interaction between the powder and liquid which is, however, so small that it could not be detected by the wet chemical method. These results are not in conflict for the nature of the phosphoric acid neutralisation curve is such that pH changes for a given degree of neutralisation are very much greater in the region of pH 4.7 than in the region of pH 2.2 (the pKa).

A similar study for C-11 showed that at all stages of the setting reaction it was a much more acid cement than C-2; at 30 min, for example, the recorded pH was 1.8 compared with 2.5 for C-2. It also hardened much more slowly. Thus the cement is strongly acidic, which is biologically undesirable, and has unfavourable hardening properties.

The changes in infra-red spectra during setting have been described in an earlier paper [6]. The data support the view that interaction between powder and liquid is very rapid once they are brought together. Rapid ionisation of H_3PO_4 to $H_2PO_4^-$ occurs at protons from the liquid exchange with glass cations, and a siliceous hydrogel is formed. In the case of C-2, infra-red evidence showed that the $H_2PO_4^-$ ions are completely removed during setting whereas C-11, even when fully hardened, was shown to contain appreciable amounts of $H_2PO_4^-$ ions which contribute to the considerable soluble fraction contained in the matrix, deduced from leaching studies to be sodium dihydrogen phosphate.

3.3. X-Ray Diffraction

All cements were found to contain a proportion

TABLE VII Diffraction data on Augelite, $Al_2(PO_4)(OH_3)$.

X-ray diffraction*		Electron diffraction†	ASTM data (14-380)‡	
d(Å)	I/I_0		d(Å)	I/I_0
4.6	W	4.56	4.67	60
4.2	W	4.05	4.27	10
			4.00	80
3.34	S	3.34	3.338	100
—	—	3.15	3.148	16
—	—	2.88	—	—
—	—	2.36	2.377	8
2.08	VVW	2.08	2.069	6
1.85	VVW	—	1.867	50
—	—	1.68	1.678	6
1.60	VW	1.59	1.595	16
1.55	VVW	—	1.544	4
			1.538	4
—	—	1.34	1.334	12

*Data from powder photographs of C-2, C-11, C-17 and C-28.
†Data from selected area diffraction of particles in a thin section of C-2.
‡Corresponding lines to those observed. Several lines recorded on the card index for which there was no experimentally observed counterpart have not been recorded.

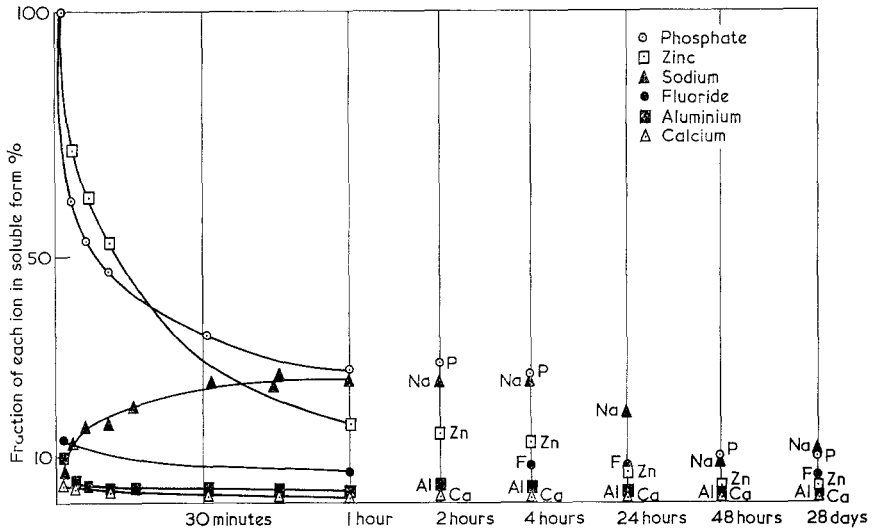

Figure 3 Variation of the soluble ion concentration with cement age (C-2).

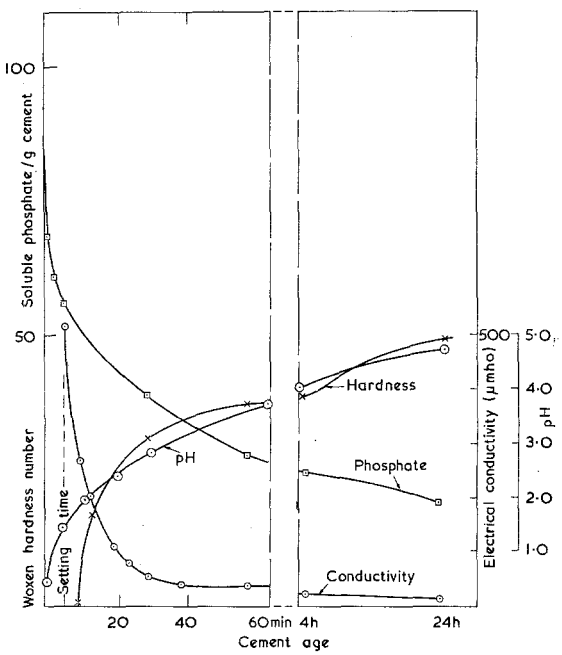

Figure 4 Variation of electrical conductivity hardness, pH, and soluble phosphate with the hardening of a cement (C-2).

of well-defined crystallites, a fact not previously established. The diffraction lines were sharp but, with certain exceptions, weak on short exposure, indicating that the amounts present were small. Two crystalline phases were detected; fluorite, CaF_2 and augelite, a basic aluminium phosphate with the composition $Al_2PO_4(OH)_3$. Cements C-6 and C-20 contained only the former, and C-17 only the latter; C-2, C-11, C-28 and C-41 contained both phases.

The identification of augelite rests on the correspondence shown in table VII between the measured interplanar spacings and those recorded in the ASTM index (card 14-380) for this phase. There appears to be some change in relative intensities and several lines to be expected were not visible. However, destructive interference or intensity changes due to solid solution or deviations from stoichiometry would be expected in view of the heterogeneous nature of the cementation reaction. That the precipitation of augelite, or a closely related species, is consistent with the chemistry of the process will be argued later and the electron diffraction data, presented in section 3.6.2, gives support to the identification.

3.4. Optical Microscopy

In reflected light, the cements appear as an irregular assembly of angular particles of greatly varying size over the range 1 to 100 μm, embedded in an apparently structureless matrix. In C-2 (fig. 5) all the glass grains could be seen to have a uniform microstructure of densely packed microspheres. In another cement, C-11 (fig. 6), this feature was only apparent in some of the grains and the microspheres, shown below by electron microscopy to be glass-in-glass phase-separated regions, were not uniform in size between one grain and another. Whether this apparent non-uniformity in microstructure in

C-11 was another factor in its being a much weaker cement than C-2 is not clear although it may be expected that differences in the distribution of ions from grain to grain in the glass particles will be reflected in non-uniform ionic distribution in the surrounding gel matrix.

A further observation, tending to support the view that irregularities in the gel may follow from variations in the glass structure, was the occurrence in the weaker cement of a well defined "reaction boundary" which tended to be associated more with those glass particles in which phase-separation was either of smaller droplet size or not visibly apparent (cf. fig. 6).

Transmission optical microscopy revealed further differences that distinguished weak and strong cements. For cements whose strengths were in excess of 173 MN/m^2, transmitted light between crossed polarisers all showed the presence of very fine birefringent crystallites which formed a network around the glass grains (fig. 7). Corresponding micrographs of the weak cements were free of all but a few sparse birefringent inclusions of coarser size.

In the case of cement C-6 the only crystalline phase identified by X-rays was CaF_2. Since this is normally isotropic, the birefringence must arise either from strain, from mutual orientation of swarms of CaF_2 crystallites whose size is comparable to the wavelength of light, from the presence of augelite crystallites too small to be identified by X-rays or from some degree of order in the amorphous aluminium phosphate short of crystallinity.

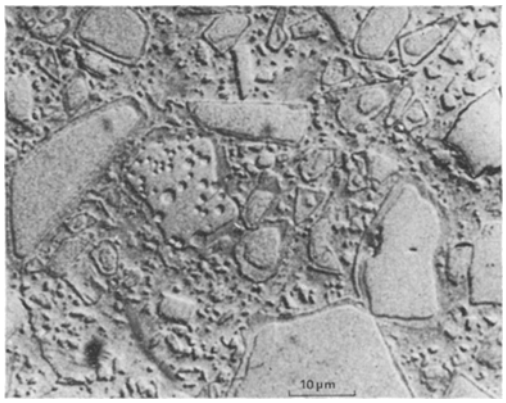

Figure 6 Reflection optical micrograph of cement C-11.

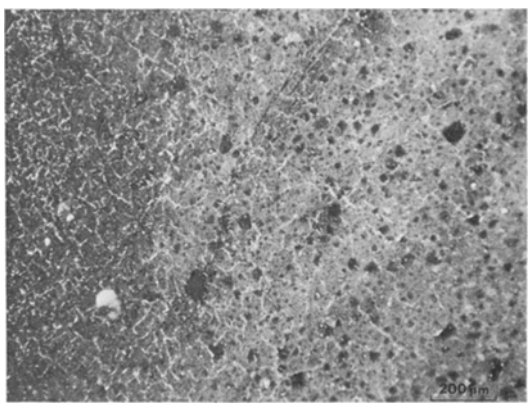

Figure 7 Transmission optical micrograph (crossed polarisers) of cement C-6.

3.5. Electron-Probe Microanalysis

The distribution of all major elements, Si, Al, Ca, Na, F and P, were studied using the special, coarse-particle cement described in section 2.2. Sodium was studied first to minimise error due to its volatility.

The electron back-scatter image photograph of the cement (fig. 8) shows that the basic geometry of the glass particles is retained in the final cement; separate particles of up to 50 × 100 μm across are distinguishable, surrounded by matrix. The almost complete absence of very fine powder results in clear definition between glass particles and matrix.

The element distribution photographs of the same area (figs. 9 to 14) show that the matrix can be clearly distinguished from the partly reacted glass particles and that the surface region of these particles is clearly defined. The differentiation of the particle from its core is shown in fig. 15 which is an optical micrograph of a study area after electron probe micro-

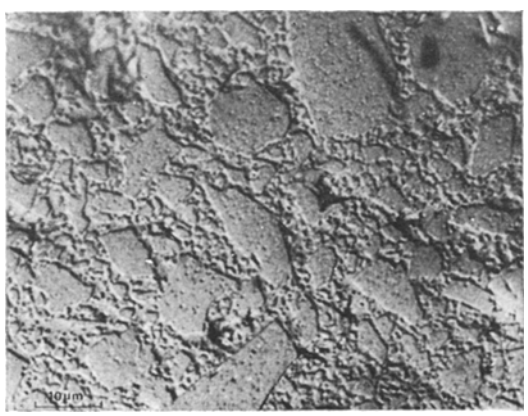

Figure 5 Reflection optical micrograph of cement C-2.

analysis. There are three geometric areas to consider: the nature of the particle core, the particle surface layer, and the gel-matrix.

The distribution photograph (fig. 9) and scan (fig. 16) for silicon shows that this element has not migrated from the particle into the matrix. The level of silicon is almost constant in the core of the particle and rises to a maximum at the interface before dropping to zero in the matrix.

Phosphorus was located almost entirely in the matrix (fig. 10) and there is no evidence of its migration into the particles. The small positive response across the particles is to be attributed to the small amount originally present in the manufactured glass.

The distributions of Al, Ca, Na and F (figs. 11 to 14) are broadly similar. Element distribution photographs (figs. 11 to 14) and scans (fig. 16) show that these elements are distributed between both particles and matrix. Their level is constant in the core of the particles but drops to a minimum in the interface region. This area of depletion coincides with the maximum recorded for silicon concentration. Since these cements were prepared using a 49% H_3PO_4 liquid containing no metal ions, it is evident that Al, Ca, Na and F (the latter probably as a cationic fluoride complex) have migrated from the surface region of the particles into the liquid phase where they form the aqueous gel matrix together with phosphorus. Aluminium phosphate has been positively identified in these cements by infra-red analysis [6] and the combined evidence suggests that an aluminium/phosphate association constitutes the major part of the continuous matrix. Less can be said about calcium, which shows a similar distribution to fluorine and is probably present as both phosphate and fluoride in the matrix. Of particular interest are the coincident maxima of aluminium, calcium and fluorine concentrations along with phosphorus in the body of the matrix. Migration from neighbouring particles results in accumulation of these ions midway between them. The precipitation process will be initiated here, resulting in a depletion of ions at this point. More ions will therefore diffuse towards this region, causing concentration minima in the neighbourhood of the particles. This is less marked with sodium since its relevant salts are more soluble and will not precipitate until later in the setting process.

The extraction of ions which is clearly taking place at the surface of the particles results in a well defined surface layer, a few microns thick, partially depleted of metal ions. This accounts for the increased silicon response at the periphery. This peripheral layer is regarded as an aluminosilicate hydrogel, and it is clear from fig. 15 that local beam-heating by the electron probe has caused moisture to evaporate and led to subsequent shrinkage. This is indicated by the darkened region. No edge contraction is shown by the unirradiated areas.

Figure 8 Electron back-scatter image photograph of cement C-2 prepared for EPMA study.

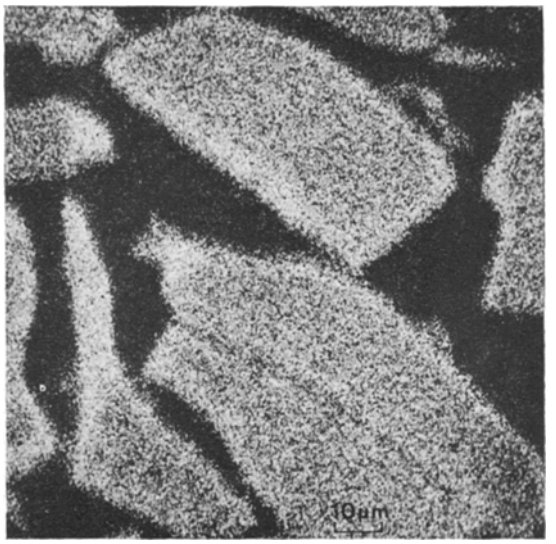

Figure 9 Element distribution photograph of silicon.

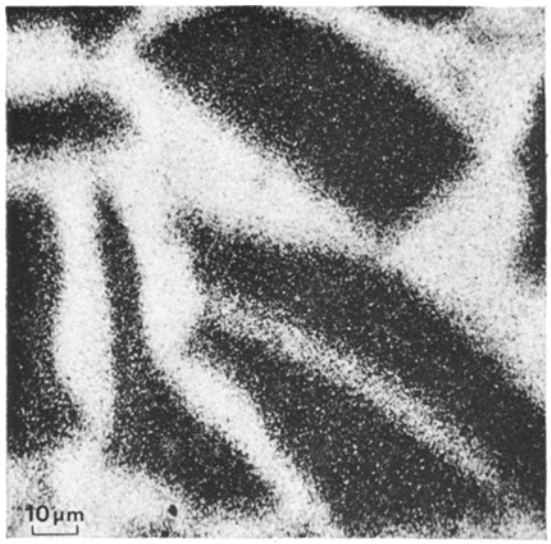

Figure 10 Element distribution photograph of phosphorus.

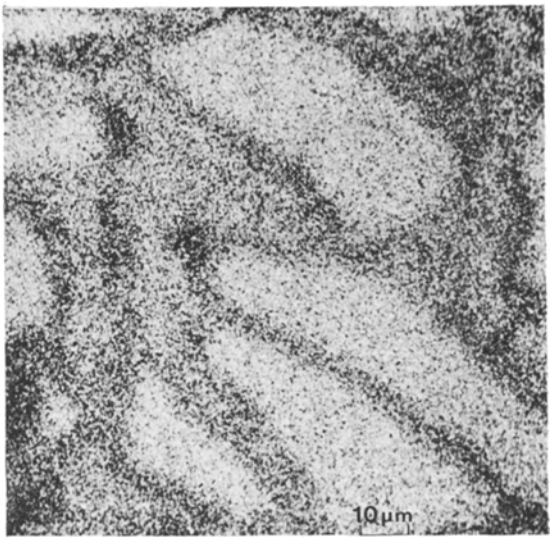

Figure 12 Element distribution photograph of calcium.

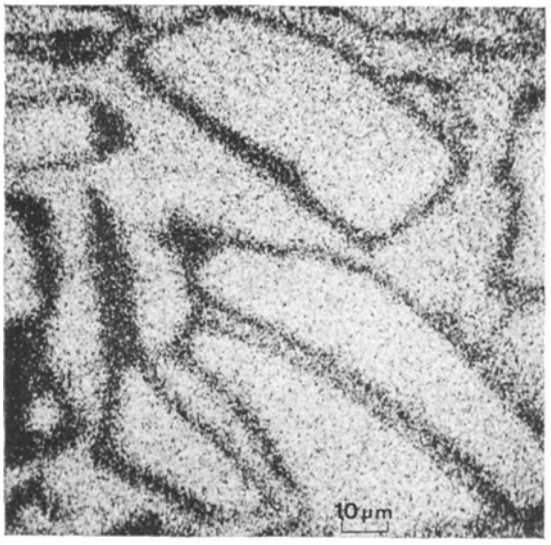

Figure 11 Element distribution photograph of aluminium.

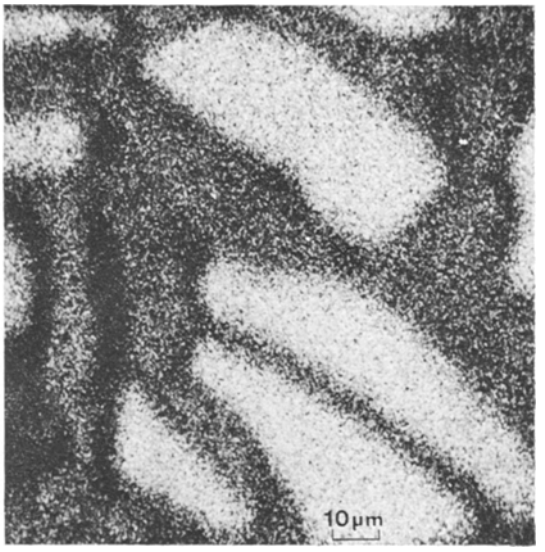

Figure 13 Element distribution photograph of sodium.

3.6. Electron Microscopy

3.6.1. The original glass

Fragments of the uncrushed original glasses were white and opal in appearance. It was evident from electron micrographs that this was due to phase-separation. The size of the droplets appeared to vary between compositions. In P-2, for example, replicas showed the segregation of droplets ~ 4000Å diameter and of much smaller regions 200 to 300Å diameter (fig. 17). Such segregation was uniform over all the glass areas studied with this composition. The shadowing on the micrographs, taken on surfaces etched for 3 sec with either 0.5% H_3PO_4 or 0.5% HF, show that the droplets, presumed to be fluorine-rich, have etched faster than the matrix. However, the flats seen in the centres of several droplets show that the dissolution of all the material in them was incomplete in the time of etching which suggests that the differential rates of attack are not great.

The phase-separated regions in P-11 contained only larger-sized droplets. Fig. 18 shows a transmission micrograph of an ion-thinned section

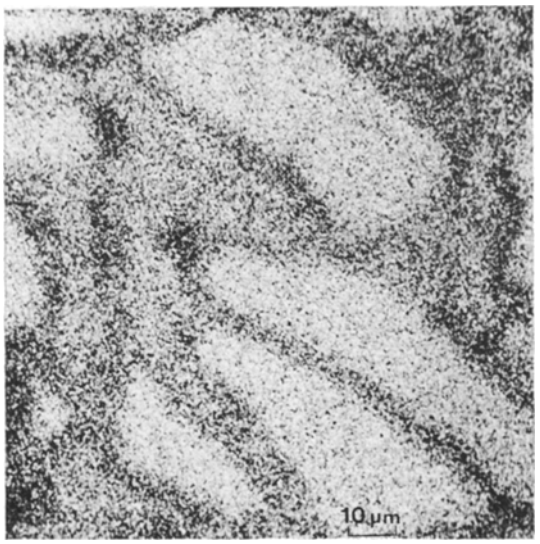

Figure 14 Element distribution photograph of fluorine.

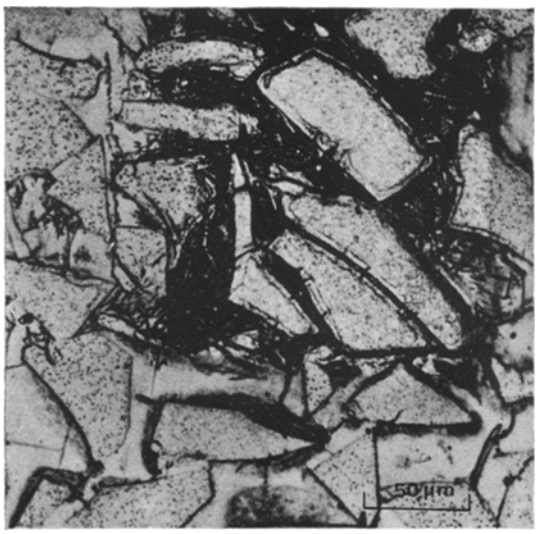

Figure 15 Optical micrograph of study area of cement C-2 after EPMA.

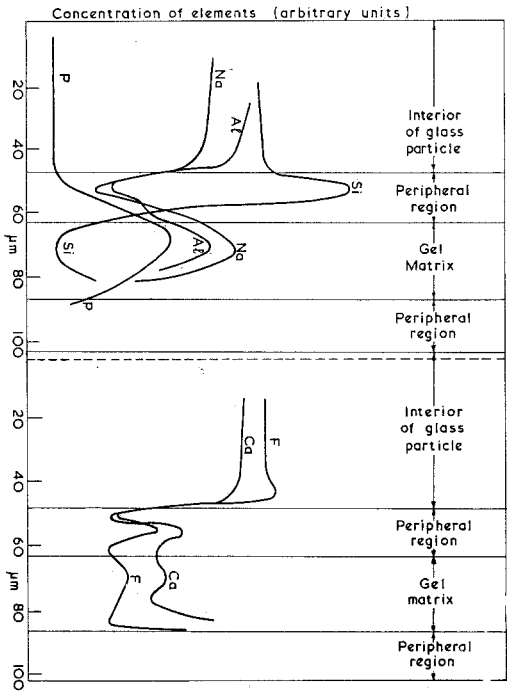

Figure 16 Element scans between glass particles and matrix.

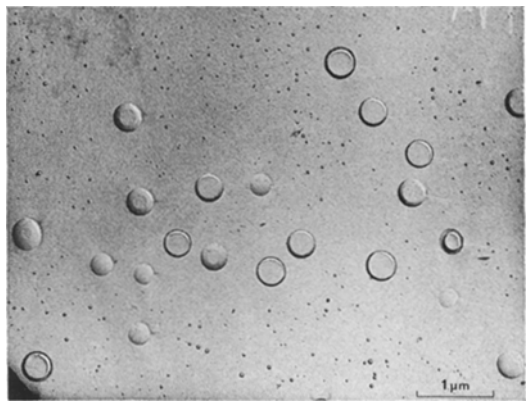

Figure 17 Electron micrograph of a single stage replica of glass P-2.

which shows droplet diameters of 2000Å. However, the optical micrographs and the electron micrographs described in section 3.6.2 show that the extent and size of these regions is not uniform in this glass.

3.6.2. The cements

In seeking differences between the microstructures of strong and weak cements, single-stage replicas were taken from fractured surfaces of C-2 and C-11. Typical micrographs are shown in figs. 19 and 20. The principal differences were apparent in the gel microstructure, which in the case of the stronger cement appeared to show a more fragmented structure with a more irregular interface at the glass grains. The replicas from the weaker cement suggested that a more continuous bond exists between the glass particles and the gel which was relatively structureless and, in the example illustrated, showed evidence of the intermediate boundary

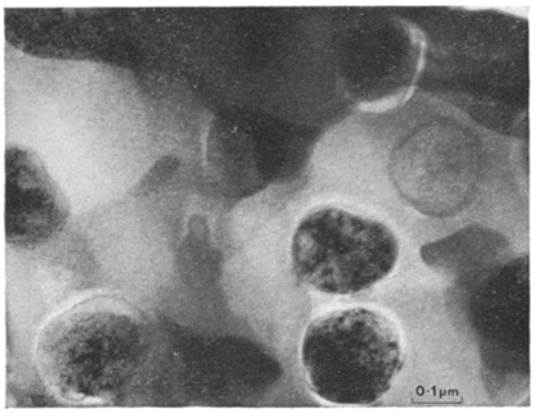

Figure 18 Transmission electron micrograph of ion thinned glass P-11.

which was also noted on the optical micrographs from this weaker cement.

A further difference, confirming the transmission optical observations, was in the degree of microcrystallinity between the two cement gels. By virtue of fortuitous adherence of pieces of cement from all regions to the carbon replicas, selected area diffraction could be used to detect and identify crystalline regions.

In the stronger cement the extraction replica of the gel matrix at high magnification could be seen to be packed with microcrystallites between 100 and 1000Å in size, identified by electron diffraction as CaF_2. Occasionally, isolated single crystals were extracted whose measured interplanar spacings from the single crystal diffraction patterns they produced corresponded to those of augelite.

Fig. 21, for example, shows such a fragment of this phase, the illuminated area being the image in dark field from the 3.34Å (220) reflection. The crystallite size of these augelite areas appeared to be between 1000Å and 1 μm. No crystallinity was detected in the extraction replicas taken from the weaker cement C-11.

At a later stage in the investigation these findings were confirmed in a more direct manner through the acquisition of the ion-beam thinning apparatus, which enabled uniform thin sections of the cements to be prepared for examination in transmission.

Figs. 22 and 23 show two areas, seen in the MEV microscope, which typify the microstructure of the strong cement C-2. In fig. 23 the area around a glass particle, in which the phase-separated droplets can be clearly seen, contains a high concentration of very small irregularly shaped particles typical of those regions giving ring diffraction patterns identifiable as CaF_2. In other areas, such as that shown in fig. 22, larger (0.5 to 2 μm) sized particles can be seen to be embedded in the gel and these gave single crystal patterns consistent with augelite. The weaker cement, C-11, appears in the MEV microscope to have a generally similar gel microstructure (fig. 24) but although it is known from the X-ray data to contain crystalline CaF_2 and augelite, areas containing these phases were rarely picked up by electron diffraction, an observation consistent with the transmission optical microscopy which showed crystallinity to be coarser and irregularly distributed.

When considering these micrographs from the MEV microscope it must be borne in mind that some morphological detail in the gel may be affected both by the ion-thinning preparation and by the MEV beam. Nevertheless the merits of these combined techniques in allowing large coherent areas of the material to be surveyed in transmission are obvious.

3.7. Scanning Electron Microscopy

The three-dimensional detail of the fracture surfaces of a selection of both weak and strong cements was explored using the Stereoscan. A brief examination of a cement whose "as-prepared" surface was visibly disfigured by crazing was also undertaken by this technique.

3.7.1. Fracture surfaces

A typical microstructure of a strong cement (C-6) is shown in fig. 25 and that of a weak cement (C-11) in fig. 26. In all cases debonding had occurred during fracture between unattacked glass particles and the matrix and it does not seem likely therefore that the strength of this bond is an important factor which might explain compressive strength differences. The most significant difference between weak and strong materials was in the gel microstructure which in the strong cements was mostly particulate, some of it presumably consisting of the crystallites described earlier. By contrast, much of the matrix material around glass grains in the weaker cements was featureless and had a more continuous platelike character.

In the case of C-6, approximately 2 wt % of glass fibre is added to the glass powder by the manufacturer, apparently on the grounds that such addition improves the set strength of the cement. It was found, however, that removal of

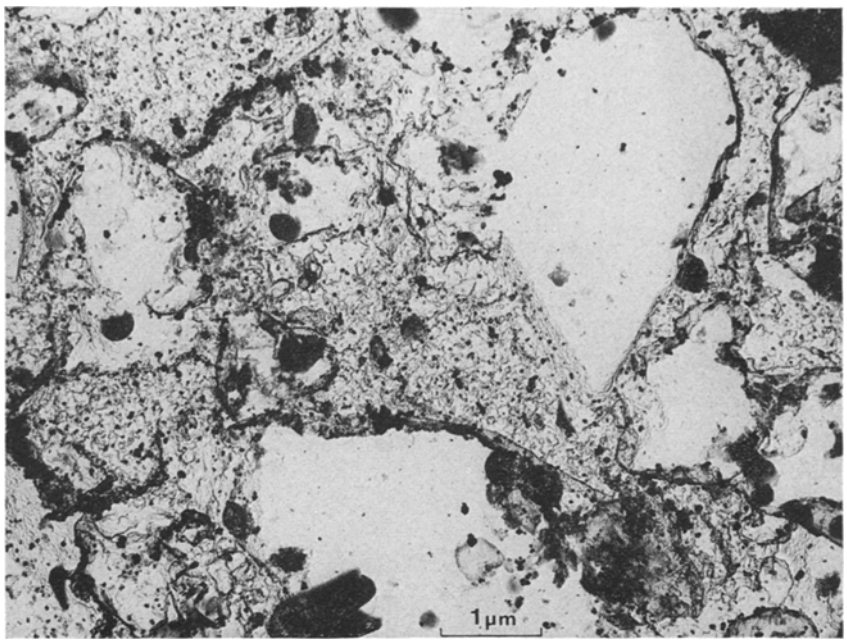

Figure 19 Electron micrograph of single stage replica of fracture surface of cement C-2.

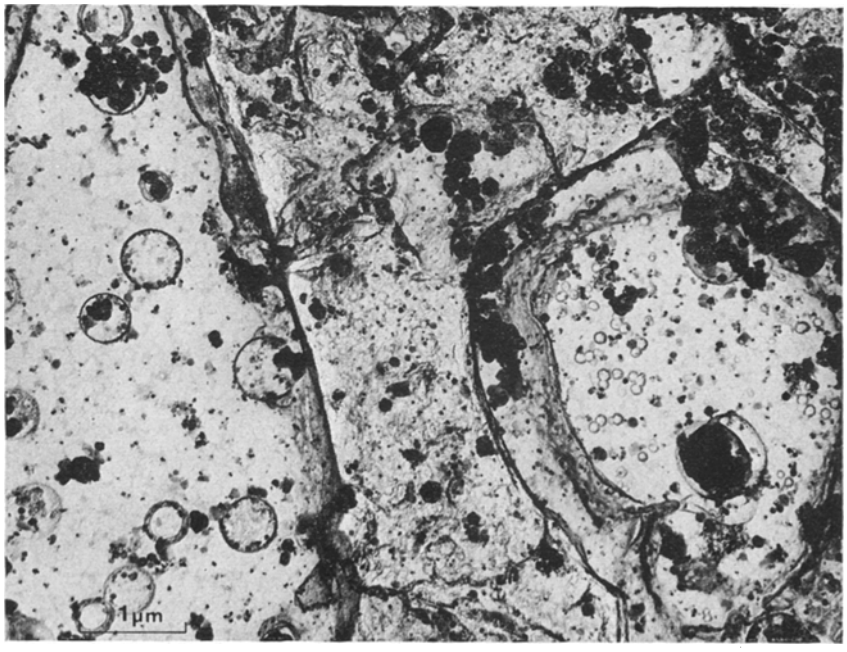

Figure 20 Electron micrograph of single stage replica of fracture surface of cement C-11.

the glass fibres before cementation improves the final strength by a factor of at least 10%. Fig. 27, which is an area containing a fibre in this cement, suggests that this is due to shrinkage away from the fibres, effectively creating a void which causes crack initiation. A brief quantitative study of the effect of fillers in dental silicate cements is described in section 3.8.

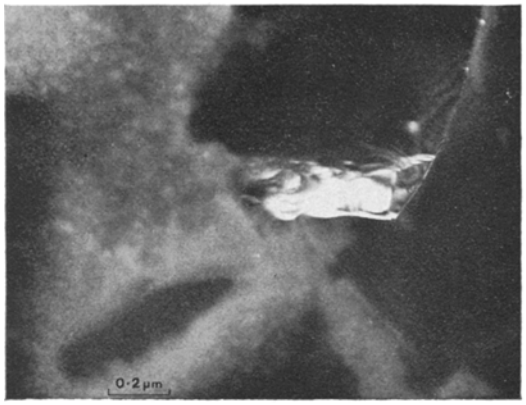

Figure 21 Extracted particle of augelite from cement C-2 illuminated in dark field.

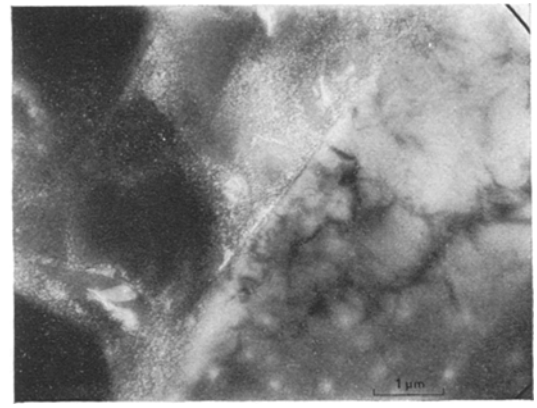

Figure 24 Transmission micrograph of ion thinned cement C-11. Photographs taken at 1000 kV using the EM7 MEV microscope.

Figure 22

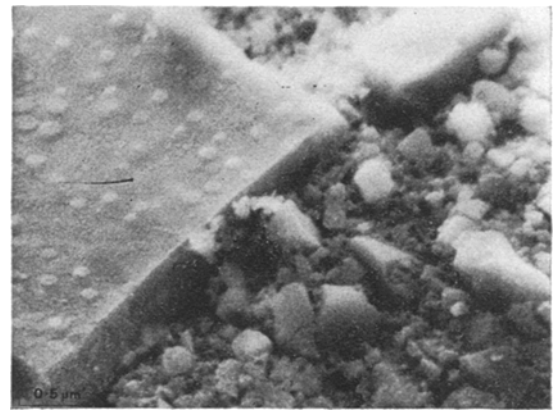

Figure 25 Stereoscan picture of fracture surface of cement C-6.

Figure 23

Figures 22 and 23 Transmission micrographs of ion thinned cement C-2. Photographs taken at 1000 kV using the EM7 MEV microscope.

3.7.2. Crazed surfaces

If the surface of a setting cement is prematurely exposed to the atmosphere, crazing becomes visible. This is aesthetically undesirable, causing an increased tendency of a filling to stain, and it causes a reduction in strength and an increase in the rate of erosion.

A severely crazed cement (C-2) was examined in the Stereoscan (fig. 28) where the surface can be seen to be pitted with 2 to 5 μm craters between which run a network of micron-sized cracks and much finer cracks. The craters and coarser cracks were also observable by optical microscopy whereas uncrazed cements under the optical microscope were smooth. However, in the Stereoscan, uncrazed cements appeared to have a network of finer cracks which presumably

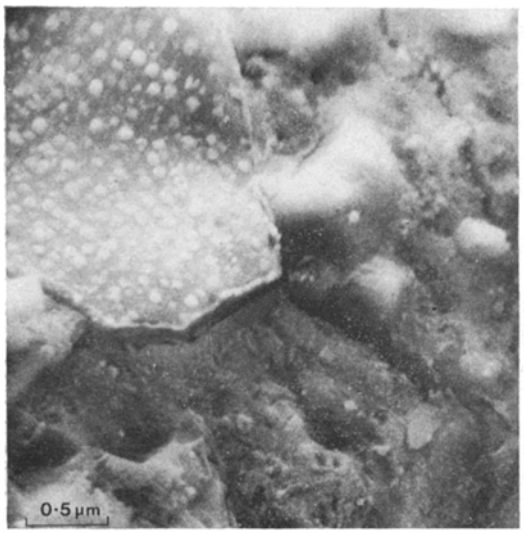

Figure 26 Stereoscan picture of fracture surface of cement C-11.

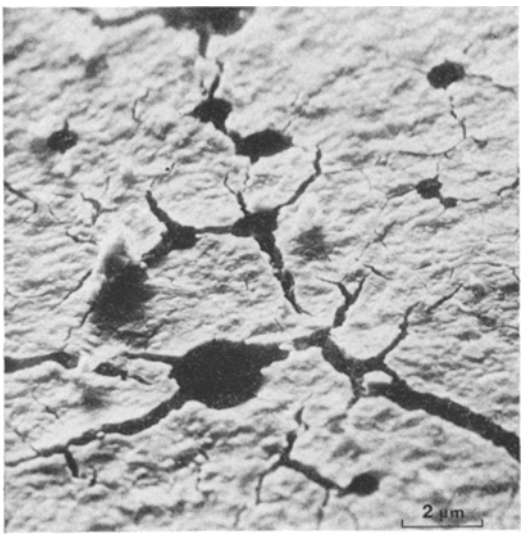

Figure 28 Stereoscan picture of a crazed surface of cement C-2.

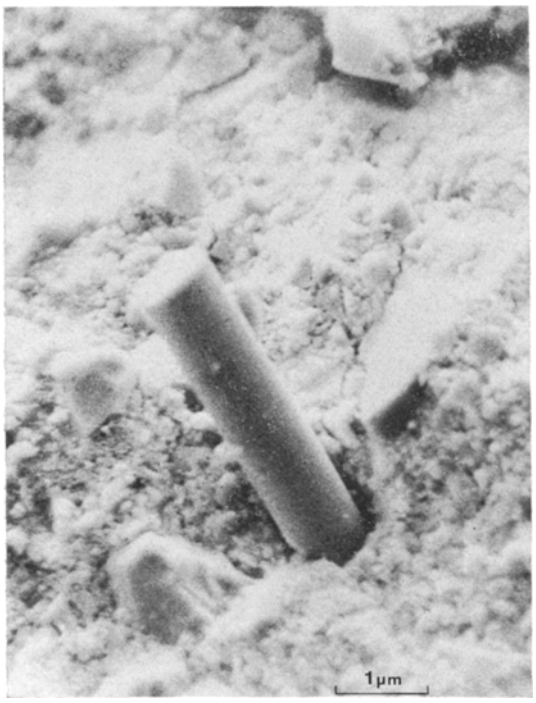

Figure 27 Stereoscan picture of an area of cement C-6 containing a glass fibre.

were an artefact induced by the vacuum conditions in the Stereoscan.

Crazing is obviously the result of certain disruptive forces exceeding the strength of the weak, brittle surface layer before it has developed its full strength.

The reasons for crazing are uncertain, although such factors as rate of moisture loss, presumably depending both on the P:L ratio used and relative humidity of the atmosphere, could be influential in causing local evaporation of liquid before it fully entered in the cementing reaction. These considerations ideally require a new filling to be immediately coated with a varnish.

3.8. Reinforcement of Dental Silicate Cements (with J. Aveston*)

Specimens of cement C-2 were prepared, using liquid: powder ratios betwen 0.35 and 0.53, and their modulus and cross-breaking strength compared with cements made at the same liquid:powder ratio, containing (a) 10 wt % of silicon carbide whiskers (− # 200); (b) 6 wt % carbon fibres (5 mm) 8 μm diameter and (c) 25 wt % Al_2O_3 powder (10 μm). The results are shown in fig. 29. They show that modulus and strength of an unreinforced cement falls as the liquid: powder ratio increases and that while there is no significant change in modulus by the addition of fillers, in some cases there is actually a decrease in breaking strength. It was not possible to make satisfactory mixes with fillers at the liquid: powder ratio commonly used (0.4) and at those ratios at which fillers could be incorpor-

*Division of Inorganic & Metallic Structure, National Physical Laboratory.

ated, the resultings cement strengths were approximately a half of that attained by unfilled drier mixes, i.e. higher P:L ratio.

Stereoscan pictures of fractured surfaces of the fibre-containing cements showed voids and cracks in the areas around the fibres similar to that shown in fig. 27, the picture of the commercial cement containing glass fibres. Similarly, the alumina particles can be seen (fig. 30) to be virtually unbonded to the cement and appear to have served no purpose except to create voids from which cracks are initiated.

The results suggest that dental silicate cements cannot be effectively reinforced by incorporation of fibres or particles, unless some means are found of effecting some adhesion between the matrix and the fibres or particles.

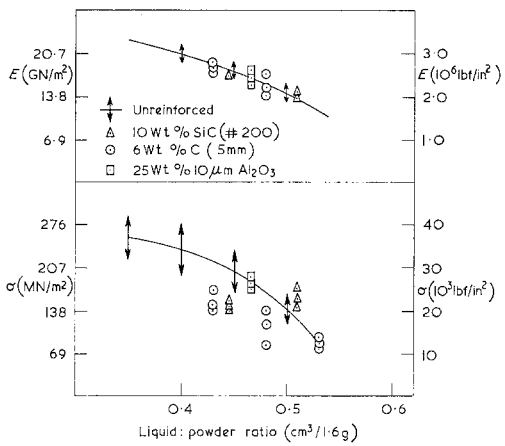

Figure 29 Modulus and cross breaking strength of cement C-2 containing fillers and prepared using different *P:L* ratios.

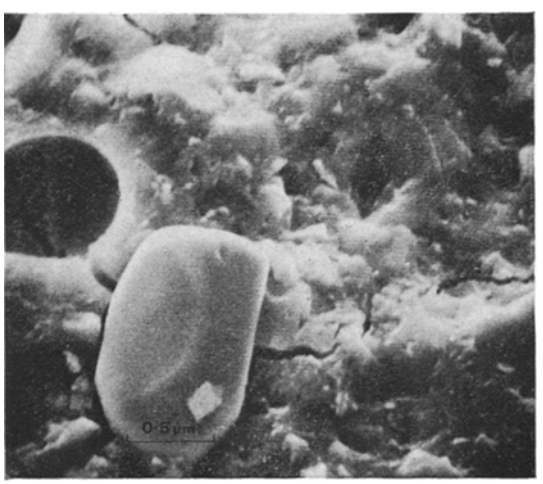

Figure 30 Stereoscan picture of cement C-2 containing alumina particle filler.

4. Discussion

A discussion on the formation of the dental silicate cement must begin by considering the physico-chemical nature of the cement forming materials.

Commercial liquids are based on phosphoric acid, a concentration of 50 wt % H_3PO_4 appearing to be optimum. In addition, most liquids contain added metals, usually a combination of zinc and aluminium. While zinc is in simple solution, aluminium forms complex monomers, dimers and polymers with phosphoric acid. The bridge structure

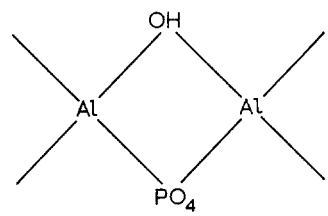

has been reported [5] and on the evidence from our work a similar association seems likely in the binding gel matrix of the cements.

Commercial powders are ground glasses and not crystalline clinkers as is usual with most cement systems. The opacity of these glasses is the result of their high fluorine content which exceeds that of all known formulations used in the opal glass industry, and causes phase-separation of fluorine-rich droplets.

The powders disintegrate readily in mineral acids which presumably break down the structure of electrophilic attack. The internal structure of these glasses is not known in detail but the main feature is almost certainly a three-dimensional network of $[AlO_4]^-$ and $[SiO_4]$ tetrahedra interspersed by droplets of a fluoride-rich phase. The overall negative charge in the continuous network part of the structure is balanced by the positive charge on the Na^+ and Ca^{2+} ions which, along with the Al^{3+} and F^- ions, will be liberated during cement formation by protons penetrating the surface layer of the glassy particles and decomposing the framework.

The infra-red evidence is consistent with the view that the glass network degrades to an aluminosilicate hydrogel which, as the results of EPMA show, remains at the periphery of the

larger particles and little or no silica migrates to the body of the gel.

The liberated ions, displaced by protons, migrate into the liquid along with fluoride ions and as the acidity of the liquid phase decreases they precipitate together with phosphate to form a cementing gel matrix.

The identification of augelite and calcium fluoride as crystalline species is in keeping with a chemical differentiation in which Ca^{2+} and F^- ions become associated preferentially and Al^{3+}, OH^- and PO_4^{3-} ions undergo a pH-dependent polymerisation. This polymerisation occurs as the $Al:H_3PO_4$ ratio and the pH increases, and gelation occurs when the complexes become insoluble.

Although speculative, a plausible model for this "solution-set" polymerisation is one in which Al^{3+} ions are bridged by OH^- and PO_4^{3-} radicals in the manner depicted earlier in the discussion and one, moreover, which would account for the failure of dental silicate cements at low pH in the mouth since depolymerisation of such a matrix by H^+ ions would readily occur.

During the process of such a setting reaction and before it is fully hardened, the cement is vulnerable to aqueous attack since many of the matrix-forming ions are in soluble form. The practical consequence of this is that a freshly inserted dental silicate cement filling needs to be protected from oral fluids by a varnish. In this way loss of binding medium and the occurrence of surface pitting and crazing can be avoided.

The present work confirms that a large proportion of the original glass particles remain unattacked and appear to act as an aggregate. In this respect there are parallels between the setting of these cements and Portland cement in which the clinker particles become bound in a gel matrix [16]. This matrix is regarded as being partially made up of an entangled mass of randomly oriented crystalline plates and splines of calcium silicate hydrates and calcium hydroxide, these having generated from the clinker particles. As a result of our observations it has been shown that in dental silicate cements a similar differentiation of the gel into some crystalline material has also occurred.

The view has been put forward [17] that tensile strength in calcareous cements is mainly due to the attractive forces between crystallites. These forces are governed by the free surface energy of the crystallites and the viscosity effects of any liquid lying between them. This second factor will reduce tensile strength, which will also be adversely affected by the presence of pores. Under compressive stress, crystallites lying at an angle to the direction of compression will slide until they come into contact with others at right angles to them after which, for further movement, the small and presumably near perfect crystallites would have to break. Their presence therefore should increase compressive strength.

On this model, the presence of pores will have a reducing influence on compressive strength which will be high compared to tensile strength, the factor, as for Portland cement, being about ten to one. Although it is not possible to draw firm conclusions, these arguments could be relevant to the case of dental silicates. It seems suggestive that only in the stronger cements are the crystallites small, numerous and regularly dispersed through the matrix. In the weaker cements the gel appears to be more continuous, platelike and crack-prone.

An earlier postulate that strength originates from a very firm bonding of unattacked glass particles to matrix material through the agency of an aluminosilicate hydrogel [13] is not fully supported by the present work. Although the EPMA results show that in both weak and strong cements an almost pure silica layer separates unattacked particles from the cation rich gel, in both types of cement the interface material is clearly only loosely bound to the glass particles and the micrographs indicate that cracks in the gel are in fact stopped at the interface by virtue of weak bonding. Any stronger linking and greater continuity could well allow the crack path to pass on through the glass and cause an even greater decrease in strength, an idea in keeping with theories on fracture toughness in composites.

When taken with the failure to effectively reinforce these cements by the addition of fillers it must be concluded from the findings reported in this paper that dental silicate cements have inherent limitations which modifications, for example to glass composition, are not likely to fully alleviate.

References

1. E. W. SKINNER and R. W. PHILLIPS, "The Science of Dental Materials", 6th Edn. (W. B. Saunders and Co, Philadelphia and London, 1967), p. 492.
2. F. A. PEYTON, "Restorative Dental Materials" (C. V. Mosby, St Louis, 1964), p. 508.
3. B. AXELSSON, *Odont Revy* **15** (1964) 150.

4. J. A. R. GENGE, A. HOLROYD, J. E. SALMON, and J. G. L. WALL, *Chem. Industr.* (1955) 357.
5. J. E. SALMON and J. G. L. WALL, *J. Chem. Soc.* (1958) 1128.
6. A. D. WILSON and R. J. MESLEY, *J. Dent. Res.* **47** (1968) 644.
7. Féderation Dentaire Internationale, Specification for Dental Silicate Cement, *Internat. Dent. J.* **11** (1961) 536.
8. R. WOXEN, *Industrial Diamond Review* **4** (1944) 241.
9. A. D. WILSON, B. E. KENT, and R. F. BATCHELOR, *J. Dent. Res.* **47** (1968) 233.
10. A. D. WILSON and B. E. KENT, *ibid* **47** (1967) 463.
11. B. E. KENT and A. D. WILSON, *ibid* **48** (1969) 412.
12. A. D. WILSON and B. E. KENT, *ibid* **49** (1970) 7.
13. *Idem, ibid*, **49** (1970) 21.
14. A. D. WILSON, B. E. KENT, R. F. BATCHELOR, B. G. SCOTT, and B. G. LEWIS, *ibid* **49** (1970) 307.
15. Council on Dental Research, *J. Amer. Dent. Assn.* **65** (1962) 428.
16. H. F. N. TAYLOR, "The Chemistry of Cements", vol. 1 (Academic Press, London, 1964) p. 20.
17. S. CHATTERJI and J. W. JEFFERY, *Nature* **214** (1967) 559.

Received 1 September and accepted 7 October 1971.